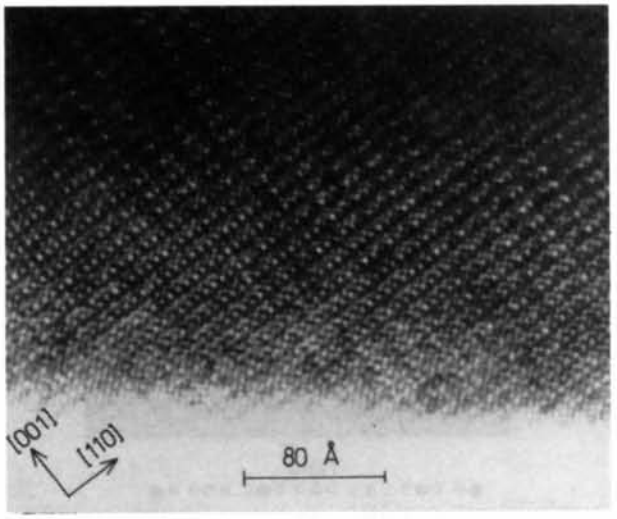

Fig. 11. Typical HREM image in ⟨110⟩. The modulations on (110) are easily seen in the thicker part of the crystal.

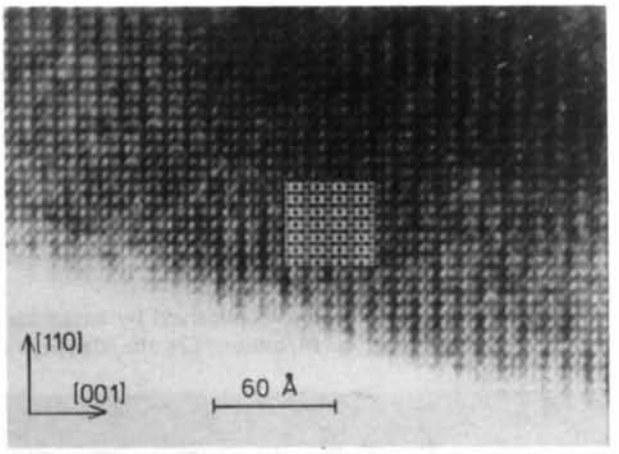

Fig. 12. Comparison between experimental and simulated image in ⟨110⟩. Defocus −90 nm. Reasonable image matching was obtained.

compatible with Al–Fe phases in the same composition range; (3) the m value is ~4·0–4·4; (4) the strongest diffraction spots are fundamental, *i.e.* most atoms scatter in phase.

From these assumptions, a framework of 126 atoms in the unit cell was set up, which produced the strongest diffraction spots. 'Vacancies' and Fe atoms were distributed in the framework by trial and error to obtain the correct 'strong' and 'weak' reflections for the other diffraction spots. The model gave qualitative, but not fully satisfying, agreement with diffraction patterns.

The model could explain the experimental HREM images, in the ⟨100⟩ as well as the ⟨110⟩ projection. This suggests that the main features of the model may be correct. On the other hand, the contrast of HREM images depended strongly on crystal thickness, questioning whether a projected structure interpretation of HREM images is applicable, even for the thinnest crystals.

In order to obtain a better structure model for Al_mFe, more experimental data, such as HREM at higher resolution, are needed.

References

ASAMI, S., TANAKA, T. & HIDENO, A. (1978). *J. Jpn Inst. Met.* **28**(7), 321–327.

BLACK, P. J. (1955*a*). *Acta Cryst.* **8**, 43–48.

BLACK, P. J. (1955*b*). *Acta Cryst.* **8**, 175–181.

COOPER, M. (1967). *Acta Cryst.* **23**, 1106–1107.

COOPER, M. & ROBINSON, K. (1966). *Acta Cryst.* **20**, 614–617.

CORBY, R. N. & BLACK, P. J. (1977). *Acta Cryst.* B**33**, 3468–3473.

MIKI, I., KOSUGE, H. & NAGAHAMA, K. (1975). *J. Jpn Inst. Met.* **25**(1), 1–9.

PORTER, D. A. & WESTENGEN, H. (1981). *Quantitative Microanalysis with High Spatial Resolution*, pp. 94–100. London: The Metals Society.

SIMENSEN, C. J., FARTUM, P. & ANDERSEN, A. (1984). *Fresenius Z. Anal. Chem.* **319**, 286–292.

SKJERPE, P. (1987). *Metall. Trans.* **18**A, 189–200.

SKJERPE, P., GJØNNES, J. & LANGSRUD, Y. (1987). *Ultramicroscopy*, **22**, 239–250.

STRID, J. & SIMENSEN, C. J. (1986). *Pract. Metall.* **23**, 485–492.

WALFORD, L. K. (1965). *Acta Cryst.* **18**, 287–291.

WESTENGEN, H. (1982). *Z. Metallkd.* **73**(6), 360–368.

Acta Cryst. (1988). B**44**, 486–494

Valence Fluctuations in the Incommensurately Modulated Structure of Calaverite $AuTe_2$

BY W. J. SCHUTTE AND J. L. DE BOER

Materials Science Centre, Laboratory of Inorganic Chemistry, Nijenborgh 16, 9747 *AG Groningen, The Netherlands*

(*Received* 15 *December* 1987; *accepted* 6 *June* 1988)

Abstract

The incommensurately modulated structure of calaverite $Au_{1-p}Ag_pTe_2$ ($p < 0·15$) with modulation wavevector $\mathbf{q} = -0·4076\,(16)\mathbf{a}^* + 0·4479\,(6)\mathbf{c}^*$, has been determined by X-ray diffraction at room temperature and at 100 K (3012 and 3017 independent reflections, respectively). The symmetry of the struc-

0108-7681/88/050486-09$03.00

ture is given by the superspace group $P^{C2/m}_{1\ s}$. The final R_F factor is 0·047 at room temperature and 0·043 at 100 K, additional temperature factor modulation lowers R_F to 0·029 and 0·035, respectively. The lattice parameters of the *C*-centered monoclinic cell are: at room temperature, $a = 7{\cdot}1947\ (4)$, $b = 4{\cdot}4146\ (2)$, $c = 5{\cdot}0703\ (3)$ Å, $\beta = 90{\cdot}038\ (4)°$; at 100 K, $a = 7{\cdot}182\ (1)$, $b = 4{\cdot}402\ (1)$, $c = 5{\cdot}056\ (1)$ Å, $\beta = 89{\cdot}99\ (2)°$. The largest displacements (about 0·4 Å) caused by the modulation are found to occur for the Te atoms. The Ag/Au ratio ($p \approx 0{\cdot}1$ for our sample) is also strongly modulated, with the silver fraction varying between 0 and 0·2. The observed modulations are interpreted in terms of valence fluctuations between Au^{I} and Au^{III}. This mechanism also clarifies the relations between calaverite ($p < 0{\cdot}15$), krennerite ($0{\cdot}20 < p < 0{\cdot}28$) and sylvanite ($p \approx \frac{1}{2}$).

Introduction

Calaverite, an important gold ore, violates in its morphology Steno's rule (Steno, 1669) of rational indices (Smith, 1902; Goldschmidt, Palache & Peacock, 1931) and has therefore attracted crystallographers' interest. Calaverite shows metallic conduction and silver-free calaverite is even superconducting at very low temperature (Meekes, 1987). Calaverite belongs to the pseudobinary system $Au_{1-p}Ag_pTe_2$ in which it is possible to substitute silver up to $p = \frac{1}{2}$. Within this system, four crystallographically different phases are known, all with the same monoclinic type of subcell. The mineral calaverite is known to have a silver content $p < 0{\cdot}15$. The mineral krennerite is found in the region $0{\cdot}20 < p < 0{\cdot}28$ and can be considered as a twin-interface-modulated long-period superstructure of calaverite (van Tendeloo, Amelinckx & Gregoriades, 1984). The mineral sylvanite is known in two forms. One form, ideal sylvanite with $p = \frac{1}{2}$, is a commensurately modulated superstructure of calaverite. The second form, with p slightly below $\frac{1}{2}$, is an incommensurately modulated structure with long-period antiphase boundaries (van Tendeloo, Gregoriades & Amelinckx, 1983*a*).

The average structures of the three minerals were solved by Tunell & Pauling (1952). They refined the structure of calaverite in space group $C2/m$ and found a monoclinically deformed CdI_2 type. They mention the so-called adventive spots, already described at length by Tunell & Ksanda (1936), but refrain from any interpretation.

It was not until 1979 that these adventive spots, now called satellite reflections, were ascribed by Sueno, Kimata & Ohmasa (1979) to 'wavy displacements' in the structure (the term 'incommensurate modulation' was not used by these authors). The satellite positions were at 27·3° from the $+c^*$ axis and 62·7° from the $+a^*$ axis, with a distance between main and first-order satellite reflections of $1/8{\cdot}3 = 0{\cdot}12$ Å^{-1}. We found this description, summarized as $\mathbf{q}_{\text{Sueno}} = 0{\cdot}40\mathbf{a}^* + 0{\cdot}54\mathbf{c}^*$, to be correct in principle, although a shorter wavevector choice, adopted below, is $\mathbf{q} = \mathbf{c}^* - \mathbf{q}_{\text{Sueno}} = -0{\cdot}40\mathbf{a}^* + 0{\cdot}46\mathbf{c}^*$, with length $1/9{\cdot}4 = 0{\cdot}11$ Å^{-1}. Unfortunately, Sueno *et al.* (1979) could not solve the structure with a sinusoidal wave-distribution function for the displacement of the Te atoms in a $5a \times 5c$ supercell approximation.

Van Tendeloo, Gregoriades & Amelinckx (1983*b*) studied calaverite by means of electron diffraction. They described the observed wavevector as slightly different from $\mathbf{q}_{\text{Sueno}}$ with a slightly different orientation (35° instead of 28° from the $\mathbf{c}^*$ axis) and with a slightly different length ($1/|\mathbf{q}| = 9{\cdot}4$ Å instead of 8·3 Å). However, from their description and from the diffraction pictures it is clear that '35° instead of 28°' should be read '−35° instead of +28°', and that van Tendeloo described not $\mathbf{q}_{\text{Sueno}}$ but $\mathbf{q}$. This interchange of vectors made him interchange $+\mathbf{a}^*$ into $-\mathbf{a}^*$ [already signalled by Dam, Janner & Donnay (1985) as a 'left-handed coordinate system'], thereby mismatching the choice of direct and reciprocal axes and causing a misinterpretation of the phenomena. Such unfortunate mismatching is a typical risk in a monoclinic structure with β very close to 90°. In such cases only reliable diffraction intensities (certainly not easy in electron diffraction), and not the diffraction geometry, are a safe guide for the axis choice. The larger intensity difference between reflections [201] and [20$\bar{1}$] in van Tendeloo's Fig. 2(*a*) could possibly have served as a warning that this indexing should be the other way round.

Pertlik (1984) published a structure determination of calaverite, with a double c axis, and with space group Pc. We have investigated 17 different natural calaverite crystals and three crystals of artificial origin, but we could not reproduce these results. However, if we assume that the author overlooked the incommensurate character of the extra reflections, his cell choice and space group are fully comprehensible. Certainly Pertlik quoted Tunell & Pauling incorrectly when saying that their adventive spots imply an axis doubling.

The morphology of calaverite was successfully solved by Dam, Janner & Donnay (1985), for the last named author certainly an elegant follow-up of his 'preliminary' publication exactly 50 years earlier (Donnay, 1935). They indexed the crystal faces with four instead of three indices, the extra index applying to $\mathbf{q} = -0{\cdot}4095\mathbf{a}^* + 0{\cdot}4492\mathbf{c}^*$. This value is in very good agreement with the $\mathbf{q}$ value determined from X-ray diffraction.

In the present paper we describe the incommensurately modulated structure of calaverite. We present the results of an X-ray analysis, up to third-order satellites, using the methods developed by de Wolff (1974) and Yamamoto (1982*a*). We show that the modulated structure is related to a strong valence

Table 1. *Lattice parameters* (Å,°) *of the average structure and the components of the modulation wavevector* **q** ($|\mathbf{q}| = 1/\lambda$) *in fractions of* **a***, **b***, **c*** ($\mathbf{a}\cdot\mathbf{a}^* = \mathbf{b}\cdot\mathbf{b}^* = \mathbf{c}\cdot\mathbf{c}^* = 1$)

Standard deviations in the last decimal place are given in parentheses

	This study		
	298 K	100 K	Tunell & Pauling (1952)
a	7·1947 (4)	7·182 (1)	7·19
b	4·4146 (2)	4·402 (1)	4·40
c	5·0703 (3)	5·056 (1)	5·07
β	90·038 (4)	89·99 (2)	90·04
q_x	−0·4076 (16)	−0·4078 (15)	
q_y	0	0	
q_z	0·4479 (6)	9·4483 (6)	

Table 2. *Numbers of reflections and R_I values for the measurements at room temperature and at* 100 K

	Observed		Unique		With $I>2\cdot5\sigma(I)$		R_I†	
	298 K	100 K	298 K	100 K	298 K	100 K	298 K	100 K
Main reflections	1180*	1489	721	709	683	707	0·041	0·077
First-order satellites	1652	1612	773	771	529	551	0·049	0·112
Second-order satellites	1589	1633	743	765	449	492	0·086	0·143
Third-order satellites	1543	1633	775	772	234	252	0·160	0·199
All reflections	5964	6367	3012	3017	1895	2002		

* The roughly 300 reflections at 298 K with $35 < \theta < 45°$ were measured in only one of the two equivalent sectors.

† $R_I = \sum_j\{N_j\sum_l[(\langle I\rangle_j - I_{l,j})^2/\sigma^2_{l,l,j}]\}^{1/2}/\sum_j[(N_j - 1)\sum_l(I^2_{l,j}/\sigma^2_{l,l,j})]^{1/2}$, where $\sum_j$ is the summation over all symmetrically independent reflections and $\sum_l^{N_j}$ is the summation over all (N_j) symmetrically equivalent reflections for unique reflection j.

fluctuation of the Au atoms. We indicate in the discussion that this mechanism also plays a role in the other compounds of the $(Au,Ag)Te_2$ system.

Experimental

Natural crystals of calaverite were obtained from Cripple Creek, Colorado. All diffraction experiments were performed with monochromatized Mo$K\alpha$ radiation on an Enraf–Nonius CAD-4F diffractometer equipped with a modified CAD-4 program (de Boer & Duisenberg, 1984). Because of the uncertainties in the literature, we investigated quite a number of different crystals, including silver-free synthetic samples, but found no principal differences amongst them, either in the cell dimensions or in the modulation vector **q**.

For the final measurements we selected a crystal with dimensions of about 0·1 × 0·1 × 0·01 mm. Lattice parameters were obtained from the positions of higher-order reflections; the modulation wavevector **q** was determined from accurately determined positions of third-order satellites. Cell constants and **q** vector, both at room temperature and 100 K, are given in Table 1. For the $I(h,k,l,m)$ intensity measurements (m is the satellite index), the crystal was always placed in such a position as to minimize absorption effects. Intensity data were collected using the θ–2θ scan method, up to $\theta = 45°$ for the main reflections and up to $\theta = 35°$ for the satellite reflections. Up to third-order satellites could be measured, higher order satellites were too weak to be observed, both at room temperature and at 100 K. In view of the low intensities, higher order satellite reflections were measured with lower scan speeds, in the ratio 6:4:3:2 for $m = 0$, 1, 2, 3, respectively. Each data-collection set was split into subsets of constant m (−3, −2, −1, 0, 1, 2, 3) and the measurement of each of these seven subsets, defined in a unique sector of reciprocal space, was followed by measurement of the equivalent sector obtained by rotation around the twofold axis. Throughout these 14 subset measurements within one data file, three intensity-control reflections were regularly monitored every 2 h and used for slight drift corrections (within ±1·5%). Including these reflections we obtained a data file of 6448 reflections at room temperature and a file of 6745 reflections at 100 K. A few second-order satellite reflections had to be removed from the room-temperature file as their intensities were influenced by the presence of a nearby main reflection. Hereafter the data were corrected for Lorentz and polarization effects and for absorption ($\mu = 650\,\text{cm}^{-1}$; transmission factors 0·09–0·52). Unique data sets were subsequently obtained by averaging equivalent reflections; for details see Table 2.

Structure determination

The usual way to describe positionally and/or occupationally modulated crystals (with wavevector **q** of length λ^{-1}) is by specifying the parameters of the positions $\mathbf{x}_0$ and/or occupation P_0 and temperature factors in the average unit cell, and by specifying for each atom μ in the nth cell the deviation with respect to the average position $\mathbf{r}_0^\mu = \mathbf{n} + \mathbf{x}_0^\mu$ and/or average occupation P_o. These deviations, $\mathbf{u}^\mu(\bar{x}_4)$ and $p^\mu(\bar{x}_4)$, are periodic: $\mathbf{u}^\mu(\bar{x}_4) = \mathbf{u}^\mu(\bar{x}_4 + 1)$ and/or $P^\mu(\bar{x}_4) = P^\mu(\bar{x}_4 + 1)$, $\bar{x}_4 = \mathbf{q}.\mathbf{r}_0^\mu$ being the fourth coordinate. The symmetry in this four-dimensional space is described by superspace groups (de Wolff, Janssen & Janner, 1981; Janner, Janssen & de Wolff, 1983). It is the aim of an incommensurate structure determination to determine the superspace symmetry and to specify, in addition to the parameters $\mathbf{x}_0$ and P_0 and the temperature factors, the displacement functions $\mathbf{u}^\mu$ and P^μ, and eventually the modulations in the temperature factors as well. We performed all refinements, both for the average structure as well as for the modulation functions, with the least-squares program *REMOS* (Yamamoto, 1982*b*), refining modulation parameters in addition to 'classical' parameters. For the average structure the *XTAL* system (Stuart & Hall, 1985) gave identical results. The modulation parameters for each atom μ, are the Fourier amplitudes $u_i^{\mu,c}$, $u_i^{\mu,s}$ ($i = x, y, z$) of the modulation

$$u_i^\mu(\bar{x}_4) = \sum_{n=1}^{N} u_i^{\mu,c}\cos(2\pi n\bar{x}_4) + u_i^{\mu,s}\sin(2\pi n\bar{x}_4),$$

Table 3. *Symmetry restrictions on the components of the modulation function*

Different results were obtained for odd- and even-order harmonics. It is indicated whether a particular component is even, odd, zero or not restricted. The origin is at $2/m$.

	Component	Odd harmonics	Even harmonics
Au/Ag	u_x,u_z	Zero	Odd
	u_y	Even	Zero
	P^{Au}	Zero	Even
Te	u_x,u_z	Zero	None
	u_y	None	Zero

and an analogous expression for $P^{\mu}(\bar{x}_4)$, with in our case $N=3$, as we observed up to third-order satellite reflections. Refinement of the variables, with one extra parameter describing the secondary extinction, was performed by minimizing R_{F^2}. The definitions of the R factors are $R_F=\sum||F_{obs}|-|F_{calc}||/\sum|F_{obs}|$ and $R_{F^2}=[\sum(|F_{obs}|-|F_{calc}|)^2/\sum|F_{obs}|^2]^{1/2}$. The atomic scattering and anomalous-dispersion factors were taken from *International Tables for X-ray Crystallography* (1974).

The symmetry of calaverite was established as follows. Starting from space group $C2/m$ for the average structure, the modulation wavevector $(\alpha, 0, \gamma)$ leads to the four-dimensional Bravais class $P^{C2/m}_{1\ 1}$. For the satellite reflections there is one systematic extinction: reflections $h0lm$ with m odd are absent. This indicates the presence of a mirror plane $(^{m_y}_{s})$ and means that the symmetry operator m_y in ordinary three-dimensional space is accompanied by a translation of $\frac{1}{2}$ in the fourth dimension. If we assume that the superspace group is centrosymmetric, an assumption

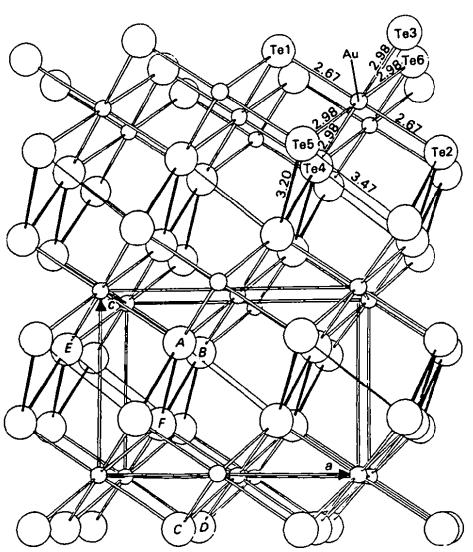

Fig. 1. Average structure of calaverite $AuTe_2$. Small circles are Au atoms, larger circles are Te atoms. Short Te–Te distances ($r_{Te-Te}<3{\cdot}3$ Å) are indicated by thick lines. Single lines indicate Te–Te distances with $3{\cdot}3$ Å $< r_{Te-Te} < 3{\cdot}7$ Å. Double lines give the Te coordination for the metal atom.

Table 4. *Final parameters of the average structure*

Standard deviations in the last decimal place are given in parentheses. At room temperature: $R_F=0{\cdot}077$ (683 reflections, 13 variables); at 100 K: $R_F=0{\cdot}087$ (707 reflections, 13 variables). The form of the anisotropic thermal parameter is: $\exp[-(\beta_{11}h^2+\beta_{22}k^2+\beta_{33}l^2+2\beta_{13}hl+2\beta_{23}kl+2\beta_{12}hk)]$.

		298 K	100 K	Tunell & Pauling (1952)
Au/Ag	x	0	0	0
	y	0	0	0
	z	0	0	0
	β_{11}	0·0039 (1)	0·0014 (1)	
	β_{22}	0·0157 (4)	0·0067 (4)	
	β_{33}	0·0097 (3)	0·0037 (3)	
	β_{13}	0·0012 (1)	0·0005 (1)	
	P^{Au}	0·86 (3)	0·86 (4)	
Te	x	0·6894 (2)	0·6890 (2)	0·689
	y	0	0	0
	z	0·2888 (3)	0·2888 (3)	0·289
	β_{11}	0·0044 (2)	0·0016 (2)	
	β_{22}	0·114 (2)	0·107 (3)	
	β_{33}	0·0093 (5)	0·0043 (5)	
	β_{13}	0·0011 (2)	0·0007 (2)	

later justified by the refinement results, the superspace group for calaverite is $P^{C2/m}_{1\ s}$, with the symmetry elements (taking the origin on $2/m$): $(0,0,0,0)$; $(\frac{1}{2},\frac{1}{2},0,0)+x,y,z,x_4$; $\quad -x,y,-z,-x_4$; $\quad x,-y,z,x_4+\frac{1}{2}$; $-x,-y,-z,-x_4+\frac{1}{2}$. This implies for our compound with $Z=2$ not only that the classical parameters are restricted [*e.g.* Au on (0,0,0) and Te on $(x,0,z)$] but that the modulation parameters are restricted as well. A list of the allowed modulation functions is given in Table 3. We see that all allowed modulations referring to the metal atom are either even or odd and that the allowed Te displacements are not restricted. Moreover, the table shows that displacements u_y come from first- and third-order harmonics and that the second-order harmonics control the displacements u_x, u_z and also the substitutional modulation P^{Au} of Au/Ag ($P^{Au}=1-p$).

We started our calculation with Tunell & Pauling's (1952) results for the average structure: Au at (0,0,0) and Te at (0·689, 0, 0·289) [the 'ideal' CdI_2-type anion positions are $(\frac{2}{3},0,\frac{1}{4})$]. The results of the refinement of the average structure (only main reflections $m=0$) are summarized in Fig. 1 and Table 4. The large temperature factor β_{22} for tellurium, together with the fact that there are large satellite intensities with increasing index k, immediately indicates a strong displacive modulation of the Te atoms along **b**. We first refined the two (sine and cosine) first-order harmonic terms of this strong Δy(Te) modulation, later followed by the one (cosine only) first-order term of Δy(Au). In due course, we added the second- (six parameters) and third- (three parameters) order harmonics for the displacement functions. Finally we added the substitutional wave (one parameter, a second-order harmonic) for the Au/Ag atom, which lowered the R_F factor for the second-order satellites from 0·157 to 0·082 and the overall R_F from 0·054 to 0·047 (room-temperature measurement). Unit weights were used for all reflections with $I>2{\cdot}5\sigma_I$ and $w=0$ for those with $I<2{\cdot}5\sigma_I$.

The final refinement results, both for the room-temperature data as well as for the measurement at 100 K, are listed in Table 5 (R factors) and Table 6 (modulation parameters).*

Eventually, we also included the temperature-factor modulations in our refinement model. This is appropriate in our case, where the large atoms see strongly changing environments owing to large modulation displacements. On the other hand, many more refinement parameters and several correlations are introduced that might not contribute to the clarity of all 'final' parameters. We therefore restrict ourselves here to a short description of the temperature modulation. At first we established, by considerations analogous to those leading to Table 3, which $\Delta\beta$ functions are allowed by symmetry. It turns out that odd harmonics contribute to $\Delta\beta_{12}$ and $\Delta\beta_{23}$ (for Te unrestricted and for the metal with odd functions only) whereas the even harmonics contribute to $\Delta\beta_{11}$, $\Delta\beta_{22}$, $\Delta\beta_{33}$ and $\Delta\beta_{13}$ (for Te unrestricted and for the metal with even functions). Therefore we expect a strong correlation between the latter modulation parameters and the substitutional parameter P^{Au}, because these are all second-harmonic effects and depend on the second-order satellite reflections only. A refinement of the room-temperature data with the first harmonic terms (six parameters) leads to a decrease of the R_F value from 0·047 to 0·042, with hardly any change in P^{Au}. Next we added the 12 second-order harmonic terms, which resulted in R_F = 0·036 and an increase of P^{Au} to 0·960 (5)–0·041 (5) $\times\cos(4\pi\bar{x}_4)$. Finally, taking the six third-order harmonic terms into account, R_F decreases to 0·029, without a further significant change in P^{Au}. The largest temperature modulation is $\Delta\beta_{22}(\text{Te}) \approx 0{\cdot}004\cos(4\pi\bar{x}_4 - \frac{1}{8})$. Another large term is $\Delta\beta_{22}(\text{metal}) \approx 0{\cdot}003\cos(2\pi\bar{x}_4)$. We find that the temperature factor of the metal is largest ($\beta_{22} \approx 0{\cdot}015 + 0{\cdot}003 = 0{\cdot}018$) at $\bar{x}_4 = 0, \frac{1}{2}$, *i.e.* at positions where the Ag content is largest, and lowest ($\beta_{22} = 0{\cdot}012$) at $\bar{x}_4 = \frac{1}{4}, \frac{3}{4}$ where the Au concentration is largest. These results are fully comprehensible because a heavier element will have a lower temperature factor. The R factors of the refinement with the temperature-factor modulation parameters are given in Table 5.

Table 5. *R_F and R_{F^2} values, and the number of parameters (np) and reflections (nr) used*

The first line corresponds to the refinement without temperature-factor modulation and the second line to the refinement with temperature-factor modulation. Numbers in parentheses, for the 100 K data, refer to values including 'less than's'.

	R_F		R_{F^2}			nr	
	298 K	100 K	298 K	100 K	*np*	298 K	100 K
$m = 0$	0·027	0·028 (0·028)	0·033	0·036 (0·036)	13	683	707 (709)
	0·023	0·027 (0·027)	0·028	0·036 (0·036)	13	683	707 (709)
$m = 1$	0·054	0·041 (0·084)	0·060	0·048 (0·088)	3	529	551 (771)
	0·027	0·035 (0·078)	0·032	0·042 (0·084)	9	529	551 (771)
$m = 2$	0·082	0·070 (0·112)	0·096	0·080 (0·114)	7	449	492 (765)
	0·040	0·048 (0·095)	0·047	0·056 (0·102)	19	449	492 (765)
$m = 3$	0·221	0·191 (0·369)	0·245	0·209 (0·339)	3	234	252 (772)
	0·110	0·106 (0·290)	0·134	0·130 (0·281)	9	234	252 (772)
All	0·047	0·043 (0·074)	0·046	0·045 (0·063)	26	1895	2002 (3017)
	0·029	0·035 (0·065)	0·031	0·040 (0·057)	50	1895	2002 (3017)

Discussion

(*a*) *Valence fluctuations as the driving force for the modulated structure of calaverite*

The average structure of calaverite is a distorted CdI_2-type structure, in which the metal atoms are surrounded by distorted octahedra of Te atoms, with two Te atoms at a distance of 2·67 Å and four at 2·98 Å. Each Te atom is surrounded by three metal atoms and five Te atoms; it is equally close to two of its five Te neighbours at 3·20 Å, with the third Te neighbour at 3·47 Å and the last two at a still larger distance of 3·77 Å. The Te atoms in the average structure form infinite zigzag chains, with interatomic distances of 3·20 Å (see Fig. 1).

As a result of the structure determination described above, we found that the real structure of calaverite is strongly modulated, with large displacements of the atoms away from the positions in the average structure. The modulation is almost independent of the temperature. From Table 6 we see that the modulation parameters at 298 and 100 K are nearly the same, and in most cases equal within the standard deviations.

In the distorted structure the nearly sinusoidal displacements of the Te atoms along **b** have an amplitude as large as 0·4 Å. A convenient way to represent these displacements (van Smaalen, Bronsema & Mahy, 1986) is to plot the Te–Te distances against the phase parameter $t = \bar{x}_4 - \mathbf{q}.\mathbf{x}_0^\mu$ of the modulation wave (Fig. 2). In most regions displacements of the Te atoms break the infinite zigzag Te chain. As a result of the displacements, there are regions in the lattice (with $t \approx \frac{1}{8}, \frac{3}{8}, \frac{5}{8}, \frac{7}{8}$) with chains on one side of the metal atom and Te–Te pairs on the other side, but in other regions ($t \approx 0, \frac{1}{4}, \frac{1}{2}, \frac{3}{4}$) only isolated Te–Te pairs (with short interatomic distances of 2·88 Å) on both sides of the metal atom are present. These are extreme cases, in fact all intermediate situations occur.

The coordination of the metal atoms by Te is also drastically modified by the modulation. The metal–tellurium distances are represented as a function of the phase of the modulation wave in Fig. 3. There are two Te atoms at a hardly modulated, short distance of about 2·67 Å from the metal atom, as in the average structure. However, the distances to the other four Te neighbours are strongly modulated. As a result the Te octahedron around a metal atom changes effectively

* Lists of observed and calculated structure factors, and temperature-factor modulation parameters have been deposited with the British Library Document Supply Centre as Supplementary Publication No. SUP 51060 (29 pp.). Copies may be obtained through The Executive Secretary, International Union of Crystallography, 5 Abbey Square, Chester CH1 2HU, England.

Table 6. *Final values for the amplitudes u of the modulation functions*

The first line corresponds to the room-temperature structure and the second line to the structure at 100 K.

	Average parameter	$\cos(2\pi\bar{x}_4)$	$\sin(2\pi\bar{x}_4)$	$\cos(4\pi\bar{x}_4)$	$\sin(4\pi\bar{x}_4)$	$\cos(6\pi\bar{x}_4)$	$\sin(6\pi\bar{x}_4)$
Au/Ag							
x	0				0·0000 (1)		
	0				−0·0001 (1)		
y	0	0·0098 (1)				−0·0051 (2)	
	0	0·0104 (1)				−0·0051 (2)	
z	0				−0·0012 (1)		
	0				−0·0017 (1)		
β_{11}	0·00381 (4)						
	0·00146 (4)						
β_{22}	0·0150 (1)						
	0·0055 (1)						
β_{33}	0·0096 (1)						
	0·00386 (8)						
β_{31}	0·00119 (4)						
	0·00053 (4)						
P^{Au}	0·905 (4)			−0·099 (4)			
	0·914 (4)			−0·089 (4)			
Te							
x	0·68935 (6)			0·0013 (1)	0·0015 (1)		
	0·68891 (5)			0·0010 (1)	0·0012 (1)		
y	0	−0·0020 (2)	0·0822 (2)			0·0067 (2)	0·0022 (2)
	0	−0·0024 (2)	0·0821 (1)			0·0065 (2)	0·0016 (2)
z	0·28833 (8)			0·0048 (2)	0·0062 (2)		
	0·28839 (7)			0·0039 (1)	0·0060 (1)		
β_{11}	0·00445 (6)						
	0·00175 (5)						
β_{22}	0·0140 (2)						
	0·0042 (2)						
β_{33}	0·0087 (1)						
	0·0038 (1)						
β_{31}	0·00069 (6)						
	0·00039 (5)						

from a linear coordination in regions $t \approx 0, \frac{1}{2}$ (see Fig. 3) with only two Te at 2·67 Å, to a square-planar coordination in regions $t \approx \frac{1}{4}, \frac{3}{4}$, with four Te neighbours at about 2·67 Å.

We will now try to understand which effects are responsible for the distinct modulated structure of calaverite. First of all we note that several transition-metal dichalcogenides have covalently bonded pairs of chalcogen atoms. Well known examples are compounds MX_2 with the pyrite structure, such as FeS_2, with Fe^{2+} ions and anion pairs $(S_2)^{2-}$. The corresponding ditelluride, $FeTe_2$, has a structure with lower symmetry, the marcasite structure with pairs of Te atoms at an interatomic distance of 2·91 Å

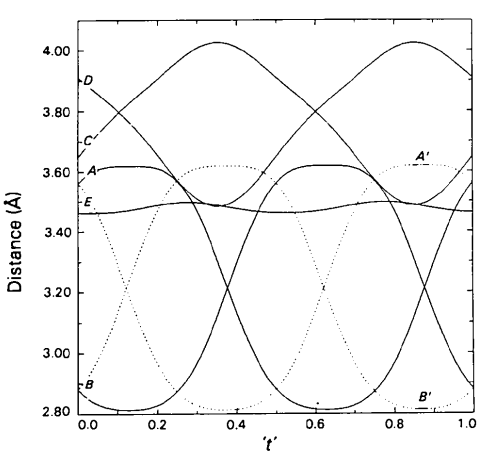

Fig. 2. Closest Te–Te distances as a function of the phase of the modulation wave at room temperature. Solid lines from Te (x, y, z) with (x, y, z) = (0·18935, $\frac{1}{2}$, 0·28833) at position F, to Te atoms at (A) ($\frac{1}{2}-x$, $y-\frac{1}{2}$, $1-z$), (B) ($\frac{1}{2}-x$, $y+\frac{1}{2}$, $1-z$), (C) ($\frac{1}{2}-x$, $y-\frac{1}{2}$, $-z$), (D) ($\frac{1}{2}-x$, $y+\frac{1}{2}$, $-z$) and (E) ($-x$, y, $1-z$). These positions are also indicated in Fig. 1. Dashed lines from Te ($-x$, $-y$, $-z$) at position $F' = -F$, to Te atoms at $A' = -A$, $B' = -B$.

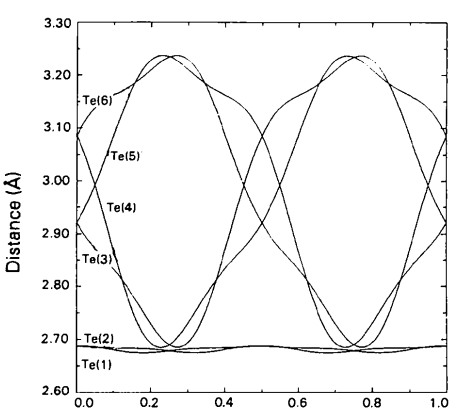

Fig. 3. Coordination of the metal atom as a function of the phase of the modulation wave at room temperature. The vertical axis gives the distance of the metal atom at (0,0,0) to Te atoms at (1) (x, y, z), (2) ($-x$, $-y$, $-z$), (3) ($x+\frac{1}{2}$, $y-\frac{1}{2}$, z), (4) ($-x-\frac{1}{2}$, $y+\frac{1}{2}$, $-z$), (5) ($-x-\frac{1}{2}$, $y-\frac{1}{2}$, $-z$), (6) ($x+\frac{1}{2}$, $y+\frac{1}{2}$, z), with (x, y, z) = (−0·31065, 0, 0·28833). For the numbering of the metal coordination see also Fig. 1. Note that the coordinates of Te(4) and Te(5) replace those from Schutte, Dam, Janner & de Boer (1987), where, following their description, they were misplaced one unit cell along **b**.

(Tengner, 1983; see Fig. 4). The Fe^{2+} ions in marcasite $FeTe_2$ are nearly octahedrally coordinated by Te, at distances of 2·57 Å.

We next discuss the relation between the electronic configuration of the metal atoms and their coordination. In calaverite we observe a continuous variation from a linear to a square-planar coordination. This might well be characteristic of Au^{I} and Au^{III}, with electronic configurations $5d^{10}$ and $5d^{8}$, respectively. Linear coordination is observed in several Au^{I} $5d^{10}$ compounds, *e.g.* AuI, Ag_3AuSe_2 (Messien & Baiwir, 1966), whereas square-planar coordination is common in Au^{III} $5d^{8}$ compounds, *e.g.* $AuCl_3$, AuSeBr (Mootz, Rabenau, Wunderlich & Rosenstein, 1973). X-ray structure determination of $Cs_2Au_2Cl_6$ reveals the presence of Au^{I} ions with a linear coordination of Au by Cl^- ions, and Au^{III} ions with square-planar coordination (Elliott & Pauling, 1938). The formula of β-AuSe could suggest the presence of Au^{II}. However, the crystal structure again shows two types of Au, with linear and square-planar coordination, attributed to Au^{I} and Au^{III}, respectively (Cretier & Wiegers, 1973). The stability of the valence fluctuation $2Au^{II}$ $5d^9 \rightarrow Au^{I}$ $5d^{10}$ + Au^{III} $5d^8$ is related to the large stability of the closed-shell $5d^{10}$ configuration and the large crystal-field stabilization of $5d^8$ in a square-planar coordination. The preference of low-spin d^8 ions for octahedral coordination is well known, and is due to crystal-field stabilization (Cotton & Wilkinson, 1980). The preference of d^{10} ions for a linear coordination is less well understood, but is presumably related to configuration interaction with d^9s states (Orgel, 1955). These considerations suggest that in the modulated structure of calaverite the electronic configuration of the Au atoms changes continuously from Au^{I} $5d^{10}$ (with linear coordination of Te) to Au^{III} $5d^8$ (with square-planar coordination). In intermediate regions there could be a mixture of Au^{I} and Au^{III} atoms, such that the average valence (averaged over a plane perpendicular to the modulation vector) is intermediate between Au^{I} and Au^{III}. However, it is also possible that in these planes there is a dynamically fluctuating valence of Au.

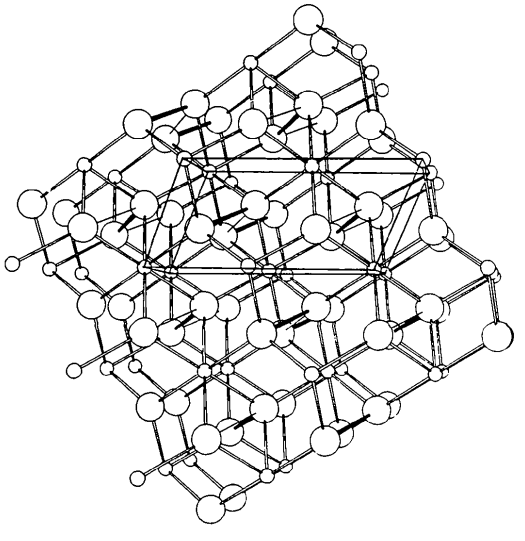

Fig. 4. Part of the marcasite-type structure of $FeTe_2$. Different types of atoms and interatomic distances are indicated in the same way as in Fig. 1. The calaverite unit cell is also indicated.

The modulation of the charge on the metal atoms influences directly the electronic configuration of the Te atoms nearby. In regions with $t \approx 0, \frac{1}{4}, \frac{1}{2}, \frac{3}{4}$, the Te–Te pairs are coordinated by Au^{I} on one side and Au^{III} on the other side. With respect to the metal atom Au^{I}, at *e.g.* $t \approx 0$, we have coordination Au^{III}–Te–Te–Au^{I}–Te–Te–Au^{III}. Here, compared to the average situation, in both Au–Te–Te–Au segments the metal has donated electrons to the nearby Te (similar to what we will see in sylvanite), thus increasing the negative charge on Te. This explains the breaking up of the Te zigzag chains in the average structure and the formation of isolated Te–Te pairs. In regions $t \approx \frac{1}{8}, \frac{3}{8}, \frac{5}{8}, \frac{7}{8}$, however, where the metal valence is intermediate between Au^{I} and Au^{III}, its coordination, at *e.g.* $t \approx \frac{1}{8}$, is Au^{I}–Te–Te–($Au^{I}Au^{III}$)–Te–Te–Au^{III}. In the second segment the metal atoms donate even more electrons to the nearby Te–Te, resulting in the formation of very short Te–Te pairs ($r = 2{\cdot}82$ Å). But in the other segment, the metal atoms take electrons from the Te–Te neighbours as compared with the average structure. This decreases the negative charge on the Te atoms, and increases the tendency for covalent bonding. This explains the persistence of Te zigzag chains with relatively short Te–Te distances ($r = 3{\cdot}20$ Å) in specific regions.

We consider briefly two mechanisms which can produce modulations in crystals. The modulated structures of many metallic transition-metal dichalcogenides (TaS_2, NbS_2, NbS_3, $NbSe_3$) are attributed to a charge-density wave mechanism (Wilson, Di Salvo & Mahajan, 1975). In these cases the distortion is caused by an instability of the conduction electrons in these highly anisotropic materials. The coupling of the charge-density wave with the lattice leads to a clustering of the metal atoms (Haas, 1985). We think that this charge-density wave mechanism is not responsible for the distortion of calaverite, because there are no metal clusters in the distorted structure.

Another effect which can be responsible for (incommensurately) modulated structures is the presence of highly polarizable atoms (Haas, 1985). In a crystal with highly polarizable anions the total energy of the crystal can be lowered by choosing a crystal structure with a very asymmetric coordination of the anions by positive ions. This is in fact the origin of the stability of the layer compounds like CdX_2 (X = Cl, Br, I) (with an asymmetric coordination of highly polarizable Cl^-, Br^-, I^- ions by three Cd^{2+} ions) compared to the structure with higher symmetry of CdF_2 (with a more symmetric coordination of the less polarizable F^- ion). The

polarization energy of the CdI_2-type structure can be increased by a further distortion, *i.e.* lowering of hexagonal symmetry, which leads to a distorted structure with even larger polarization energy. One expects and indeed finds such distorted layer structures, especially for the ditellurides MTe_2 (M=Mo, W, Nb, Ta, V) with highly polarizable Te ions. The electric polarization of Te will certainly contribute to the stability of the average structure of calaverite, and perhaps also to that of the modulated structure.

(*b*) *The effect of* Ag *in the structure of mixed compounds* $Au_{1-p}Ag_pTe_2$

Strong support for the proposed valence fluctuations of the Au atoms comes from a careful consideration of the behaviour of Ag-substituted crystals. It is well known that in (nearly) all stable compounds Ag is monovalent Ag^{I} $4d^{10}$; Ag^{II} $4d^9$ and Ag^{III} $4d^8$ are quite unstable. Therefore one expects that Ag substitution will take place only for Au^{I} (*i.e.* in regions $t\approx 0, \frac{1}{2}$), and not for Au^{III} (regions, $t\approx\frac{1}{4}, \frac{3}{4}$). This is precisely what is found in Ag-substituted calaverite (see Table 6): the silver content $p = 1 - P^{Au} = 1 - [0{\cdot}9 - 0{\cdot}1\cos(4\pi\bar{x}_4)]$ which has a maximum, as $\mathbf{x}_0^{Au} = 0$, at $t\approx 0, \frac{1}{2}$, and is zero at $t\approx\frac{1}{4}, \frac{3}{4}$. This may even explain the low solubility limit ($p\approx 0{\cdot}15$) of Ag in calaverite; above a certain concentration it is no longer possible to substitute Ag for Au. The modulated structure of calaverite is stable at least in the range $0 < p < 0{\cdot}15$. $AuTe_2$ ($p = 0$) already has an incommensurate modulation. The direction and length of the modulation vector hardly change as a function of the Ag content, p, but it does change in direction and length when part of Te is substituted by Se (van Tendeloo *et al.*, 1983*b*).

We now compare the structure of calaverite with that of sylvanite $AuAgTe_4$, depicted in Fig. 5. The structure of sylvanite is described by Tunell & Pauling (1952) in space group $P2/c$, with one Au, one Ag and two independent Te atoms in the unit cell (Fig. 5). A more convenient description (van Smaalen, 1987), with a smaller number of parameters, is provided by the same superspace group as used for calaverite and a modulation wavevector $\mathbf{q} = (-\frac{1}{2}, 0, \frac{1}{2})$. In this description in terms of a commensurate modulation, there is only one independent metal atom and one independent Te atom, with four different values ($t = 0, \frac{1}{4}, \frac{1}{2}, \frac{3}{4}$, see Fig. 6) of the phase of the modulation wave. The 180° phase shift ($t = \frac{1}{2}$) is equivalent to the c glide in space group $P2/c$. The 90° phase shift ($t = \frac{1}{4}$) represents the second independent Te atom in the $P2/c$ description. The correct Ag/Au distribution in sylvanite is determined by the condition that only a second-order modulation of the occupation of metal sites exists. The structures of sylvanite and calaverite are very similar. Also in sylvanite the six neighbours of each metal atom are at the vertices of a strongly distorted octahedron. Each Au atom has two Te neighbours at 2·67 Å, two at 2·75 Å and two at a much larger distance of 3·25 Å. The four neighbours at 2·67 and 2·75 Å lie in a plane at the corners of a parallelogram which is nearly a square. Each Ag atom has two Te neighbours at 2·69 Å, two at 2·96 Å and two at 3·20 Å, the two neighbours at 2·69 Å forming a linear coordination of Ag. This again represents a situation where the d^{10} atom (here Ag^{I} $4d^{10}$) has a linear coordination, and the d^8 atom (Au^{III} $5d^8$) has a square-planar coordination.

In sylvanite there are Te pairs with Te–Te distances of 2·87 Å. These pairs are also seen (Fig. 2) in the modulated structure of calaverite at $t = 0, \frac{1}{4}, \frac{1}{2}, \frac{3}{4}$. The structure of sylvanite can be compared to the structure of marcasite $FeTe_2$ (Tengner, 1938) which also shows Te pairs (distance 2·91 Å), see Fig. 4. The main difference between marcasite and sylvanite is the metal coordination. In marcasite all metal atoms Fe^{II} are octahedrally coordinated by Te, in sylvanite the coordination is linear (Ag^{I}) or square planar (Au^{III}). In

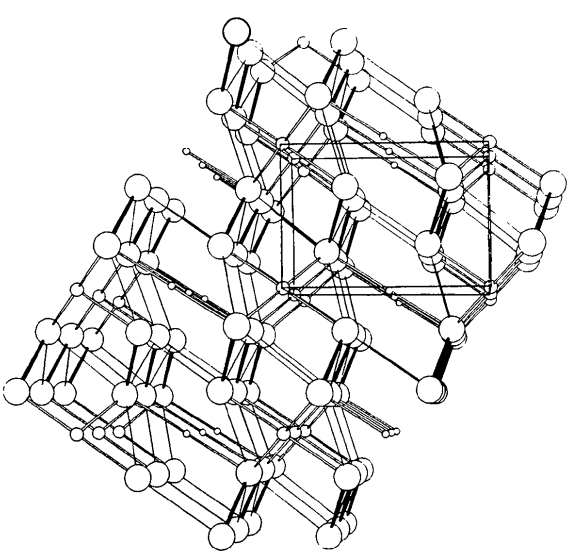

Fig. 5. Part of the structure of sylvanite (Tunell & Pauling, 1952). Interatomic distances are indicated in the same way as in Fig. 1, Te atoms are represented by large circles, Ag atoms by small circles and Au atoms by medium-sized circles. The calaverite unit cell is indicated.

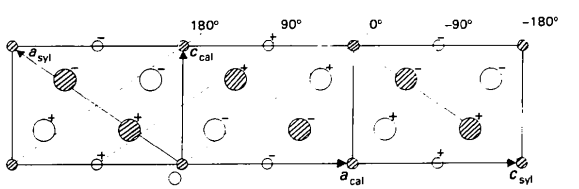

Fig. 6. Structure of sylvanite, projected on the [010] plane as a commensurate modulated structure with the same subcell as calaverite and with Au on the origin. The dotted lines indicate wavefronts, numbers give the relative phase shifts of the modulation wave. Small circles indicate metal atoms, large circles indicate Te atoms; the open circles are at $y = \frac{1}{2}$, while the shaded circles are at $y = 0$. The atoms marked with + are displaced upwards and those marked – are displaced downwards.

sylvanite the Ag and Au atoms are arranged asymmetrically around the Te atom, the Ag on one side, the Au on the other side (providing maximum polarization in an ionic model).

Compounds with a higher Ag content ($p > \frac{1}{2}$) than is present in sylvanite have not been reported. These compositions are probably not stable at ordinary temperature and pressure, as they would involve Ag in a higher oxidation state. When substituting Au for Ag in sylvanite ($p < 0{\cdot}5$) the distribution of Au^{I} and Au^{III} leads to an incommensurately modulated structure with the same modulation vector as in calaverite. Periodic antiphase boundaries are also present in this structure; along these boundaries excess gold can be incorporated in the crystal (van Tendeloo *et al.*, 1983*a*). For even higher concentrations of Au ($0{\cdot}20 < p < 0{\cdot}28$) the krennerite structure is formed (Tunell & Pauling, 1952). In this structure half of the Te atoms form pairs, the others are divided into isolated Te atoms and distorted Te chains. This structure is a complicated twinned-interface commensurate superstructure (van Tendeloo *et al.*, 1984) with a monoclinic subcell, and with the twin plane parallel to the $[10\bar{1}]$ plane (*i.e.* parallel to the plane of constant phase in calaverite and the antiphase boundary plane in sylvanite). The Au and Ag atoms are ordered, with Ag preferentially located along the twin interface.

Concluding remarks

The present X-ray analysis shows that calaverite $Au_{1-p}Ag_pTe_2$ ($p \approx 0{\cdot}10$) has an incommensurately modulated structure with superspace group $P^{C2/m}_{1\ s}$ and modulation wavevector $\mathbf{q} = -0{\cdot}4076\mathbf{a}^* + 0{\cdot}4479\mathbf{c}^*$. The displacements of the atoms in the modulated structure with respect to the average structure are large, which shows that the modulation has a major effect on the structure. Large displacements of the Te atoms effectively vary the coordination of the metal atom from linear to square. The modulation of calaverite is caused primarily by a valence fluctuation of the Au atoms, between Au^{I} with a linear coordination of Te, and Au^{III} with a square-planar coordination. This valence fluctuation induces the strong modulations of the Te lattice, the breaking up of the zigzag chains and the formation of isolated Te pairs. These effects also make it possible to understand the other phases and structures of sylvanite and krennerite in the ternary system $Au_{1-p}Ag_pTe_2$.

This work is part of the research program of the Netherlands Foundation for Chemical Research (SON) and was made possible by financial support from the Netherlands Organization for the Advancement of Pure Research (ZWO). We thank Dr Ruth Pitt, Boston, for kindly supplying natural calaverite crystals and Dr S. van Smaalen and Professor C. Haas for stimulating discussions.

Note added in proof: A consistent and complete description of the morphology of calverite is given in Janner & Dam [*Acta Cryst.* (1988), A**44**. In the press].

References

BOER, J. L. DE & DUISENBERG, A. J. M. (1984). Enraf–Nonius CAD-4F diffractometer software, updated February 84. Groningen, Utrecht, The Netherlands.

COTTON, F. H. & WILKINSON, G. (1980). *Advanced Inorganic Chemistry*, 4th ed., p. 647. New York: Wiley–Interscience.

CRETIER, J. E. & WIEGERS, G. A. (1973). *Mater. Res. Bull.* **8**, 1427–1430.

DAM, B., JANNER, A. & DONNAY, J. D. H. (1985). *Phys. Rev. Lett.* **55**, 2301–2304.

DONNAY, J. P. H. (1935). *Ann. Soc. Geol. Belg.* **18**, B222.

ELLIOT, N. & PAULING, L. (1938). *J. Am. Chem. Soc.* **60**, 1846–1851.

GOLDSCHMIDT, V., PALACHE, C. & PEACOCK, M. (1931). *Neues Jahrb. Mineral. Geol. Palaeontol. Abh. Abt. A*, **63**, 1–58.

HAAS, C. (1985). *J. Solid State Chem.* **57**, 82–96.

International Tables for X-ray Crystallography (1974). Vol. IV. Birmingham: Kynoch Press. (Present distributor Kluwer Academic Publishers, Dordrecht.)

JANNER, A., JANSSEN, T. & DE WOLFF, P. M. (1983). *Acta Cryst.* A**39**, 671–768.

MEEKES, H. (1987). Private communication.

MESSIEN, P. & BAIWIR, M. (1966). *Bull. Soc. R. Sci. Liege*, **35**, 234.

MOOTZ, D., RABENAU, A., WUNDERLICH, H. & ROSENSTEIN, G. (1973). *J. Solid State Chem.* **6**, 583–586.

ORGEL, L. E. (1955). *J. Chem. Phys.* **23**, 1005–1014, 1824–1826.

PERTLIK, F. (1984). *Z. Kristallogr.* **168**, 227–236.

SCHUTTE, W. J., DAM, B., JANNER, A. & DE BOER, J. L. (1987). *Acta Cryst.* A**43**, C-312.

SMAALEN, S. VAN (1987). *Acta Cryst.* A**43**, 202–207.

SMAALEN, S. VAN, BRONSEMA, K. D. & MAHY, J. (1986). *Acta Cryst.* B**42**, 43–50.

SMITH, H. (1902). *Mineral. Mag.* **13**, 125.

STENO, N. (1669). *De Solido intra Solidum Naturaliter Contento.* Florence: Star.

STUART, J. M. & HALL, S. R. (1985). *The XTAL System of Crystallographic Programs*, 2nd ed. Tech. Rep. TR-1364.1. Computer Science Center, Univ. of Maryland, College Park, Maryland, USA.

SUENO, S., KIMATA, M. & OHMASA, M. (1979). *Modulated Structures* 1979, AIP Conf. Proc. 53, edited by J. M. COWLEY, J. B. COHEN, M. B. SALAMON & J. WUENCH, p. 333. New York: American Institute of Physics.

TENDELOO, G. VAN, AMELINCKX, S. & GREGORIADES, P. (1984). *J. Solid State Chem.* **53**, 281–289.

TENDELOO, G. VAN, GREGORIADES, P. & AMELINCKX, S. (1983*a*). *J. Solid State Chem.* **50**, 335–361.

TENDELOO, G. VAN, GREGORIADES, P. & AMELINCKX, S. (1983*b*). *J. Solid State Chem.* **50**, 321–334.

TENGNER, S. (1938). *Z. Anorg. Allg. Chem.* **239**, 126–132.

TUNELL, G. & KSANDA, C. J. (1936). *J. Wash. Acad. Sci.* **26**, 507–528.

TUNELL, G. & PAULING, L. (1952). *Acta Cryst.* **5**, 375–381.

WILSON, J. A., DI SALVO, F. J. & MAHAJAN, S. (1975). *Adv. Phys.* **24**, 117.

WOLFF, P. M. DE (1974). *Acta Cryst.* A**30**, 777–785.

WOLFF, P. M. DE, JANSSEN, T. & JANNER, A. (1981). *Acta Cryst.* A**37**, 625–636.

YAMAMOTO, A. (1982*a*). *Acta Cryst.* A**38**, 87–92.

YAMAMOTO, A. (1982*b*). *REMOS*82.0. Computer program for the refinement of modulated structures. National Institute for Research in Inorganic Materials, Sakura-mura, Niihari-gun, Ibaraki 305, Japan.